CARBON 66 (2014) 154–163

Available at www.sciencedirect.com

ScienceDirect

journal homepage: www.elsevier.com/locate/carbon

Self-heating fiber reinforced polymer composite using meso/macropore carbon nanotube paper and its application in deicing

Hetao Chu [a], Zhichun Zhang [a], Yanju Liu [b], Jinsong Leng [a,*]

[a] Center for Composite Materials and Structures, No. 2 YiKuang Street, Science Park of Harbin Institute of Technology (HIT), Harbin 150080, PR China

[b] Department of Aerospace Science and Mechanics, No. 92 West DaZhi Street, Harbin Institute of Technology (HIT), Harbin 150001, PR China

ARTICLE INFO

Article history:
Received 16 May 2013
Accepted 23 August 2013
Available online 5 September 2013

ABSTRACT

A meso/macropore carbon nanotube paper (CNP) and a self-heating fiber reinforced polymer composite of CNP/glassfiber/epoxy (CGE) based on the meso/macropore CNP were fabricated in this article. The pore diameters mainly distribute from 30 to 90 nm characterized using nitrogen adsorption isotherms at 77 K. The electric conductivities of the CNP and CGE composite are 77.8 and 64.9 S cm^{-1}. Electric heating performance of CGE was investigated at different heat flux densities, wind speed and ambient temperature. A uniform temperature distributed was observed on the surface of CGE detected by an infrared temperature camera. The electric heating performance was verified by deicing a certain amount of ice at different heat flux densities under two kinds of ambient conditions: −22 °C without wind and −22 °C with 14 m/s of the wind speed. The deicing time under the two conditions were less than 220 and 450 s, respectively. The feasibility of the deicing performance was demonstrated through a series of experiments and the results indicate this material is a promising candidate as an electric heating material for deicing.

1. Introduction

Recently, the use of composites has significantly increased in the past few decades, for instance the composite material proportion has reached 50% of the total weight in the Boeing 787. In many cases, icing inevitably occur on the surfaces of aircraft, such as freezing rain falling on them or the leading edge of the wing freeze when aircrafts flight alternating between hot and cold airflow. This phenomenon causes a serious safety risk to pilots and aircraft. Hence, many deicing strategies have been used to mitigate the effects of ice on aircraft. Among these deicing methods, deicing salts are mainly adopted to solve the problem. However, most of deicing salts contain chloride and have a strong tendency to cause corrosion and pollute groundwater although are inexpensive and effective [1,2]. Given this problem, other deicing strategies utilizing electric thermal technique also have been developed. Generally speaking, thermal technique can be categorized as internal heating that the heat is generated by internal component and transferred by a good thermal conductor to the outer surface, for example electric cable and carbon fiber heating wire, and external heating using microwave and infrared heating [3]. It is difficult to achieve the target by the internal heating method for polymer matrix composites, because polymer always possesses poor thermal conductivity and if employs the external heating method, it brings a number of difficulties to maintain the aerodynamic shape of the aircraft. So it is necessary to study a self-heating fiber reinforced polymer composite.

* *Corresponding author:* Fax: +86 451 86402328.
E-mail address: lengjs@hit.edu.cn (J. Leng).

0008-6223/$ - see front matter
http://dx.doi.org/10.1016/j.carbon.2013.08.053

Carbon nanotube paper (CNP) is a non-woven fibrous structural film entangled assemblies of carbon nanotube (CNT) with 2D paper-like morphology held together by Vander Waals forces between CNT junctions [4] as ordinary paper made from wood pulp fiber [5–7]. Typical methods used to produce the CNP are filtration [8], Langmuir–Blodgett deposition [9], CVD growth [10] and CNT/polymer composite [11,12]. Generally, CNP exhibits unusual multi-functionalities of flexibility, high thermal conductivities [13], and electrochemical activity [14]. Thus, CNP has widely been used in the distillation devices, sensor, actuator, fire retardants, field emission displays and filtration [15–25]. In view of the tremendous potential application of CNP, a large body of experimental and computational works aimed at exploring their various properties. Cao et al. [16,17] reported that single-walled carbon nanotubes (SWCNT) CNP can hold as an active material for various electronic and sensor system applications. Chen et al. [17] synthesized aligned CNP using aligned CNT in the presence of a magnetic field. They found that aligned CNP demonstrated stable and fast responses under the open air in the absence of electrolytes. Xu et al. [26] found that the CNP demonstrates frequency and temperature-invariation viscoelasticity from −196 to 1000 °C. Che et al. [27] reported CNP as freestanding electrodes for super capacitors by co-packaging CNP with conducting polymer and thermosetting resin. Currently, most of the researches mainly focus on the application of free-standing CNP, as they still have severe limitations in terms of product quality, especially mechanical properties, because CNP always are not strong enough to composite with other materials and should be carefully handled during fabrication.

In this work, a self-heating composite of meso/macropore CNP-glassfiber-epoxy (CGE) for deicing was proposed for the first time. The CGE composite was fabricated by a series of steps utilizing meso/macropore CNP as the functional layer and glassfiber as the mechanical reinforcement layer. The electric heating performance of the composite was tested at different heat flux densities, wind speed and ambient temperature; investigated by deicing quantitative ice under two kinds of ambient conditions: −22 °C without wind and −22 °C with 14 m/s of the wind speed. The meso/macropore CNP used in this paper was fabricated by suspension filtration. Due to the continuous nanotube networks, CNP usually has a higher conductivity and low volume resistance than the CNT-polymer composites. The low-dimensional and pores make epoxy penetrate through the maze/macropore CNP forming an interspersed structure. The conductivity of resulting material is much higher than CNT-polymer composites as previous report [28–33]. The results indicate the self-heating composite is a promising candidate as an electric heating material for deicing.

2. Experimental

2.1. Materials

Purified SWCNT used in this study were purchased from Chengdu Organic Chemicals Co., Ltd., Chinese Academy of Sciences. The nanotubes have an average outer diameter of 1–2 nm and individual tube lengths range from 5 to 30 μm synthesized by a chemical vapor deposition with carbon content more than 90 wt%. Commercially available bisphenol A type epoxy resin (EX-2511–1A, ShangWei Wind Power Material Co., Ltd., China) with an average viscosity of 900–1400cps and a density of 1.15 cm^{-3} at 25 °C was used as a matrix. As a curing agent, an amine type hardener (EX-2511–1BS, ShangWei Wind Power Material Co., Ltd., China) was used. Epoxy resin utilizing in this article contains a constant weight ratio (10:3) with the curing agent and cure at room temperature. In order to prevent entanglement of the SWCNT and to obtain a better dispersion, polyoxyethylene octylphenylether (Triton X-100, Biochemical grade, Aladdin Chemical Reagents Co., Ltd., China) was employed as a nonionic surfactant in fabricating CNP. The Polyimide (PI)-kanthal electric heating film used in the experiment was commercially available.

2.2. Measurements

Scanning electron microscopy (SEM) observations were performed using a Quanta 200F Field-Emission Scanning Electron Microscope (FE-SEM) with an operating voltage of 30 kV.

Digital microscopy characterization was studied on KEYENCE (VH-Z500R) microscope system.

A contact angle test was carried out using a microscopic Contact Angle Measurement (OCA20, GFR), at room temperature. The characterization was used to demonstrate the spread capacity of the epoxy resin on the surface of meso/macropore CNP.

Conductivity was measured using a Napson Resistivity Measurement System (RG-7C) Four-Point Probe with 0.4 mm probe tip diameter and 1.0 mm tip spacing.

Nitrogen adsorption isotherm measurement was analyzed by a Micrometrics ASAP 2020 volumetric adsorption analyzer at 77 K. The Brunauer–Emmett–Teller (BET) method was used to calculate the specific surface area and average pore size of the CNP.

Electric heating performance of CGE composite was detected by an infrared temperature camera (VarioCAM® HiRes sl, JENOPTIK Infra Tec.).

2.3. Fabrication meso/macropore CNP and introduce electrodes

CNP was fabricated by multiple steps of SWCNT dispersion and suspension filtration. Typically, 1 g SWCNT were mixed with 5 g Triton X-100 and dispersed by three roller shear disperser (DS50, EXAKT) for 20 min. Then, the paste-like mixture was dissolved in 5 L deionized water and the solution dispersed by dynamic sonication using a high-power ultrasonic processor (Vibra-CellTM, Sonics) circulation twice resulting in a stable and homogeneous solution. After that this stable solution was infiltrated through a filter element covered by a membrane with a pore size of 1 μm to form the CNP. Subsequently, the as-prepared CNP was treated at 90 °C for 5 h and peeled from the filter membrane.

A commercial copper foil was used for the electrodes in the experiment with the size $120 \times 2 \times 0.03$ mm^3. The connection between the electrodes and the CNP was achieved

utilizing a conductive carbon nanotube adhesive (Carbo e-Therm LT, Future Carbon).

2.4. Molding fabrication self-heating composite of CGE

Fig. 1 schematically illustrates the proposed assembly process of fabricating CGE composite, which involves two processes of presoak and molding cure. To further package the SWCNT network with epoxy, firstly, CNP was presoaked with epoxy (3 wt% in ethanol) for 2 h at room temperature to introduce the resin to penetrate into the inner space and enwrap the individual SWCNT or SWCNT bundles. Then the resulting prepreg was degassed in a vacuum atmosphere for 30 min. Subsequently, the prepreg composited with glassfiber and epoxy by compression molding for 24 h under 0.5 MPa to make it contact with epoxy resin integrally. Finally, a self-heating composite was fabricated successfully in the size of $120 \times 100 \times 1.5$ mm^3 containing 1.45 wt% SWCNT and 35 wt% glassfiber. The infiltration and package processes of the CNP layer are shown in the magnified areas. Resin infiltrated into the homogeneous structure and SWCNT were wrapped with epoxy molecular chains formed a model analogous neural network, and then further packaged with epoxy to form a multilayer structure. The PI-kanthal film was fabricated with epxoy using the same method as CGE composite. The comparison image of the two sample is presented in Fig. S1.

3. Results and discussion

3.1. Characterization of SWCNT meso/macropore CNP

The gross visual appearance of the as prepared CNP is exhibited in Fig. 2(a) with the size of $180 \times 270 \times 0.07$ mm^3. Apparently, the surface is smooth and has a little metallic luster. The insert photo of CNP plane indicates it is flexible enough to be manipulated as the ordinary paper. Fig. 2(b) and (c) are the FE-SEM micrographs of the surface and partial enlargement of the CNP. These pores in Fig. 2(b) indicate a porous CNP was constructed. It is clear that SWCNT bundles are randomly distributed on the surface forming complicated homogeneous networks and the surface is slightly uneven distinguished by the change of reflecting light. Furthermore, SWCNT bundles contact closely between each other resulting in a denser film due to self-assembly by Vander Waals forces, electrostatic forces, π–π interactions between the CNT and physical cross link points. Fig. 2(c) shows homogeneous networks of SWCNT bundles with pore diameter ranging from ten nanometers to tens of nanometers and many clear physical cross link points. The network is hierarchical and looks a bit like a reticulated branching network connected by these cross link points. The interactions between SWCNT in the network offer a pathway for electron transport through the film. Thus, the CNP has excellent conductivity, strength and flexibility which permit it to be manipulated like traditional carbon fiber sheets as an electric heating element.

The pore structure and surface feature of SWCNT CNP were investigated by nitrogen adsorption isotherms at 77 K as demonstrated in Fig. 3. The pore diameter distribution curve was obtained from nitrogen Barret–Joyner–Halenda (BJH) dV/dlogD adsorption isotherm. Obviously, a wide pore diameter distribution range is revealed in this curve and the meso/macropore characteristic is displayed. In addition, two peaks can be easily found in the broad distribution range, which mainly approach at about 3.3 and 46.6 nm and the large portion of pores ranging from 30 to 90 nm is considered to be formed by empty spaces created intermingled long bundles. The porosity is conducive to spread of the epoxy resin on the surface of CNP. It is observed from the contact angle test, insert image in Fig. 3(a), where epoxy resin droplet forms a contact angle of 23.1°at room temperature.

As can be seen from the Fig. 3(b), the sample basically followed the type IV isotherm with H_1 hysteresis loop. Therefore, the as-prepared CNP can be seen as a uniform pore structure and the H_1 hysteresis loop is the evidence that the as-prepared CNP is an ordered mesoporous materials and a more steady uptake of N_2 at a medium relative pressure (0.3–0.8) and abrupt of N_2 at the high relative pressure (above 0.9). The mesoporous ensures that the permeability of the resin to penetrate through the thickness direction and maximum maintain the compactness with the CNP. From the insert curve of Fig. 3(b), a slow increase of N_2 uptake below $P/P_0 = 0.1$ suggests that almost no micropore exist in the material.

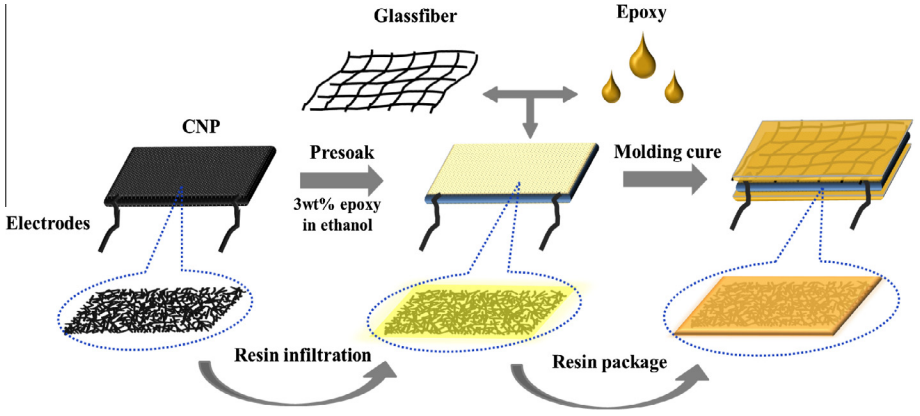

Fig. 1 – The fabricating process of CGE composite. Magnified areas are the schematic drawing of the CNP at different stages. (A colour version of this figure can be viewed online.)

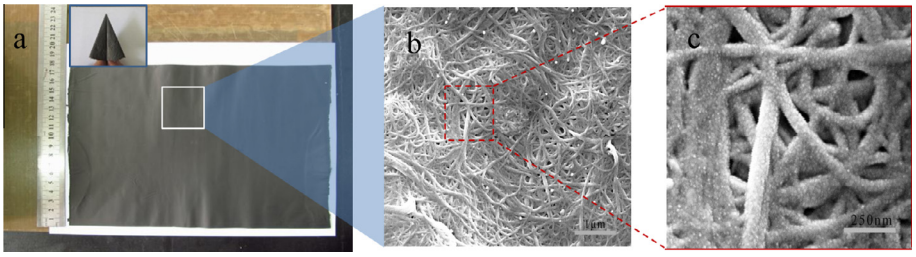

Fig. 2 – (a) Dimensions digital pictures of as-prepared meso/macropore CNP; the inset image is a plane using the resulting CNP to display the outstanding flexibility as ordinary paper. (b) FE-SEM image of the meso/macropore CNP observed on the top. (c) Partially enlarged photo of Fig. 2 (b). (A colour version of this figure can be viewed online.)

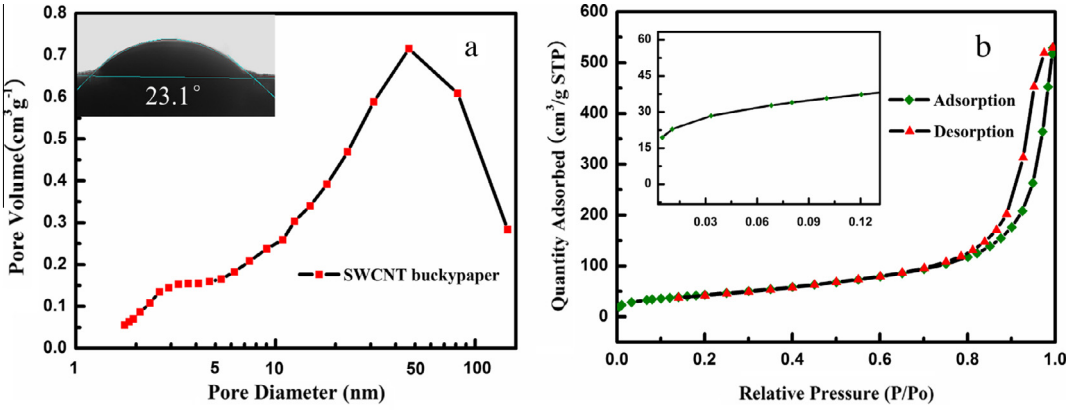

Fig. 3 – (a) Pore size distribution of the as-prepared meso/macropore CNP; the insert photo is the contact angle of the epoxy utilizing in this article on the surface of meso/macropore CNP at room temperature. (b) Adsorption and desorption isotherm of the CNP, the insert illustration is the partial amplification curve. (A colour version of this figure can be viewed online.)

3.2. *Cross section analysis of CGE composite*

Fig. 4 shows the cross section of the self-heating composite with containing 1.45 wt% SWCNT and 35 wt% glassfiber. The samples of Fig. 4(a) and (b) were treated with mechanical abrasion using 2000 mesh sand paper, and a clear multilayer structure with epoxy-CNP-glassfiber-epoxy was fabricated successfully. The electric heating layer of the CNP and the glassfiber layer are fully combined with epoxy. The thickness of the CNP is about 70 μm with a more distinct photo shown in Fig. 4(b). The glassfiber plays two roles in the CGE composite, on the one hand, the mechanical strength of the composite is greatly improved by adding glassfiber layer to meet the requirement for practical application, i.e. the fields of aircraft and wind turbine blade; on the other hand, it is proposed as a thermal-insulated layer because of its favorable insulting and poor thermo-conductive properties. So that the heat generated by CNP layer can be transmitted to a single direction.

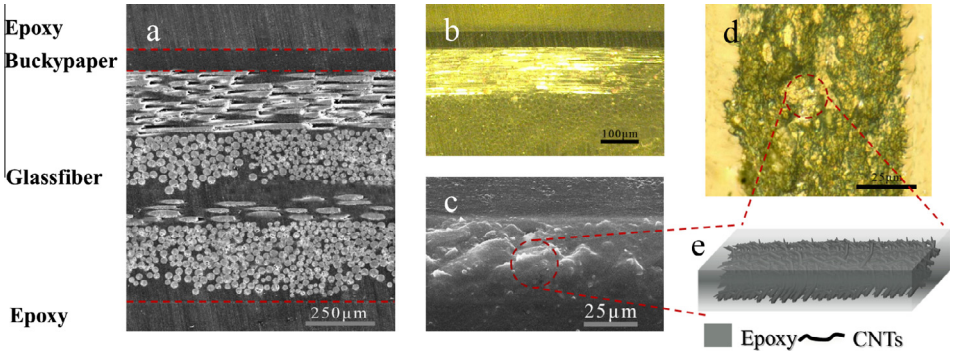

Fig. 4 – (a) FE-SEM micrograph of the cross section after polishing of the CGE composite. (b) Optical photo of the cross section after polishing with a distinct interface of CNP layer and the thickness is about 70 μm. (c) FE-SEM micrograph of the CNP layer. (d) Optical photo of the CNP layer, alternative bright and dark represents resin and CNT. (e) Schematic diagram of a repair-concrete structure. (A colour version of this figure can be viewed online.)

Fig. 4(c) and (d) are the magnified images of the CNP layer with the samples brittle fractured at low temperature in order to observe the inner structure. Compared to the as-prepared CNP shown in Fig. 2 before resin infiltration, CNP is surrounded by curing epoxy resin as shown in Fig. 4(d). In addition, the fracture surface is rough and exists some massive particles on the cross profile in the red circles. This demonstrates the CNP layer has good toughness because the SWCNT formed complicated networks and embedded in the epoxy resin. The most important is that such a continuous structure not only reduces the interface effect, which a key parameter to evaluate the performance of the composite materials, but also improves the conductivity sharply of the CGE composite. The electrical property will be analyzed in the following characterization.

To further confirm the presence or absence of epoxy resin in the CNP layer, optical microscopy image was carried out on the cross section of the sample as shown in Fig. 4(d). It can be seen that the CNP layer has large amounts of yellow crystalline block epoxy resin particles distributing through the thickness direction in the red circle as the same particles in Fig. 4(c). This means the resin infiltrate into the inner space of the meso/macropore CNP and SWCNT bundles are fully packaged by the resin forming the mixture crystalline particles. A schematic diagram is demonstrated in Fig. 4(e), in order to explain more details about the interesting structure. The homogeneous CNT networks embeds into the continuous phase of the resin as a conductive layer and the continuous phase maintains the mechanical properties of CGE composite. The mass and dimension data of CGE composite and the internal CNP layer are summarized in Table 1. It is obvious that the addition of the CNP almost does not increase the quality of the CGE composite.

3.3. *Electrical and electric heating properties of CGE composite*

3.3.1. *Conductivity analysis of the as-prepared CNP and CGE composite*

The electrical conductivity was measured using the conventional four probe technique; the resistance between the electrodes was carried out on a highly sensitive resistance meter and the results are presented in Table 2. According to the previous work, CNT-based CNP conductivities are in the range of 2–200 S m^{-1} [34,35].

As shown in Table 2, the conductivity of CNP does not have a significant variation compared with the CNP layer in the CGE composite, in spite of the fact that epoxy around the SWCNT bundles is insulating. This means that the conductive path for electron in the SWCNT network is not impeded by the processes of resin infiltration and resin package. Thus, the polymer coating only wraps on the surface of SWCNT bundles and does not disturb the intra-bundle junctures and the physical cross link points because the junction resistance between nanotubes dominates the overall electrical transport (high tube–tube contact resistance) compared with the internal resistance of nanotubes [28].

Table 1 – Physical characterization of the CGE composite and the internal CNP.

Sample	Mass (mg)	Density (g cm^{-3})	Size (mm^3)
CGE composite	17.0	1.42	$120 \times 100 \times 1$
CNP	0.25	0.42	$120 \times 100 \times 0.07$

Two other facts are clearly revealed in these data. On the one hand, CNP layer resistance has emerged a small increase after being fabricated as CGE composite, just increasing by 0.3 Ω between the electrodes. This demonstrates that the tube–tube contact without damage when the resin penetrated though pores, which is a significant step in preparing conductive CGE composite. In order to comprehend the structure more clearly, the resistance of the network morphology can be described using a random resistor network model. The assumption in the model is that the electrical resistance along SWCNT is much lower than the junction resistance so that the CNP network can be illustrated by a series of resistors ideally connected by the bundles or individual SWCNT. In addition, the strong π–π interactions between the CNT make the tube–tube bind tightly and the shrinkage of the wrapping network leads to a further tight binding of the CNT. On the other hand, the conductivity of CGE composite increases nearly four orders of magnitude than the literature focused on the conductivity of CNT–epoxy composite with the similar CNT mass fraction [28,33]. The two facts indicate that the conductive network maintains a good connection when the resin sufficiently infiltrated into the CNP.

Most of the conducting polymer composites are typically by embedding conductive particles in an insulating matrix. Generally, the resulting materials often exhibit low conductivity because the CNT are isolated by the insulating matrix and cannot form a pathway for electron transportation. To some extent, these conductive materials cannot be used as electrical heating material. Nevertheless, the CGE composite solves the problem through offering a continuous network to increase the conductivity dramatically and this method has never been reported, especially when it performs in a self-heating composite for deicing.

3.3.2. *Electric heating performance analysis of the CGE composite*

Fig. 5(a) shows the rising process of the average surface temperature of the sample under different voltage from 4 to 12 V (interval is 2 V and latter is the same) corresponding to the heat flux densities 358, 808, 1442, 2583 and 3733 W/m^2 with the analysis rectangle area R4 shown in Fig. 6(b). The balance values of these curves on the y axis are the equilibrium temperatures on the surface and these inflection points crossing with the dashed line on the x axis are the time to the equilibrium temperature. As can be seen from the figure, the equilibrium temperature of the sample increases gradually as the heat flux density increases and the required time for equilibrium temperature becomes larger gradually. Furthermore, at the beginning, the temperature dramatically increases in a short period of time, implying that, CGE composite displays excellent electric heating performance as shown in previous similar study [36,37]. According to Fig. 5(b), it is obvious that the equilibrium temperature increases gradually at different heat flux densities while the heating rate nearly accelerates

Table 2 – Electrical conductivity of CNP and CGE composite contrast with the reference.

Sample	Electrical conductivity (S cm^{-1})	CNT fill content (wt%)	Resistance between electrodes (Ω)
SWCNT	1.0×10^4	—	—
CNP	77.8	—	3.3
CGE composite	64.9	1.45	3.7
Pure epoxy	Insulation	—	—
CNT-epoxy composite [33]	1.0×10^{-2}	1.0	—

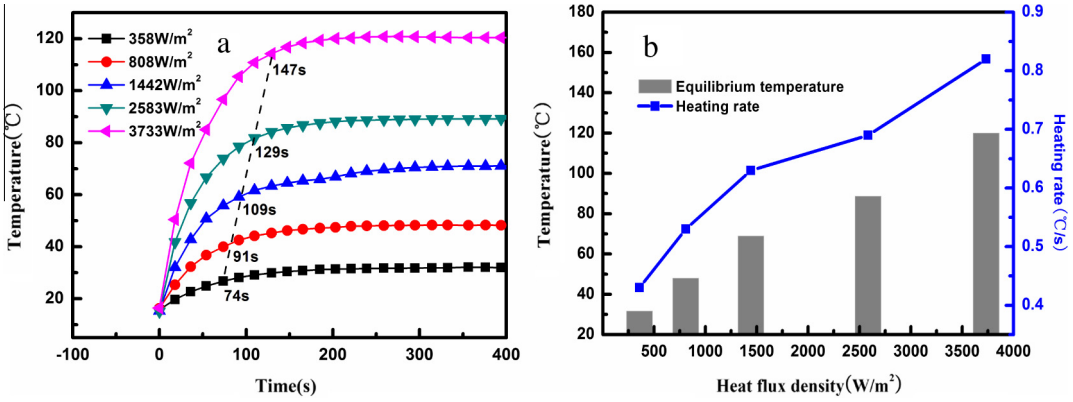

Fig. 5 – (a) The electric heating process curves of the rectangle R4 in Fig. 6(b) at different heat flux densities. (b) Column graph of equilibrium temperature and heating rate curve at different heat flux densities. (A colour version of this figure can be viewed online.)

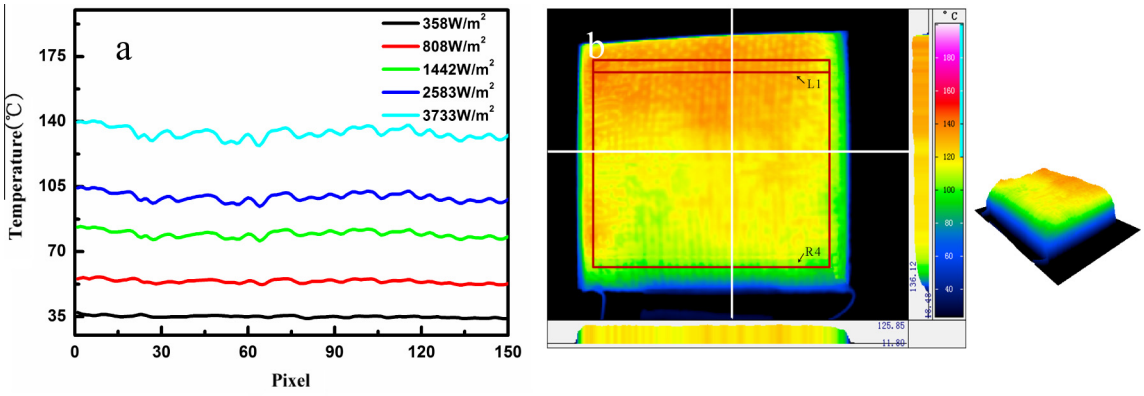

Fig. 6 – (a) Line temperature distribution curves at different flux densities. (b) 2D (left) and 3D (right) surface temperature distribution photos. (A colour version of this figure can be viewed online.)

to double with the heat flux densities increasing from 358 to 3733 W/m^2. The high heating rate means that CGE composite is suitable for deicing because, in general, electrical heating materials for deicing are required to reach a high temperature in a short time.

From the Fig. S2(a), the equilibrium temperature is almost the same of the two samples at each heat flux density. However, the times of ramping up stage (Fig. S2(b)) as Fig. 5(a) are shorter than PI-kanthal film composite and from the tendency of the linear fit, the increments of the equilibrium time of CGE composite are less than PI-kanthal film composite as the increase of heat flux densities. This suggests CGE has the faster temperature response than PI-kanthal film. Therefore, CGE requires less energy than PI-kanthal film to achieve the same temperature, because the area of the rectangle surrounded by heat flux density, x axis and y axis is the consumed energy. The advantage of the CNT film heaters is intensified by their emissivity close to unity [38] as well as uncommonly small heat capacity [39]. The fast temperature response and less energy consumption are very promising for deicing applications.

In order to discuss the temperature field distribution, line temperature and surface temperature distribution were carried out on the sample. Fig. 6(a) is the line temperature distribution at different heat flux densities of L1 in Fig. 6(b). The results indicate that the temperature fluctuation on the line

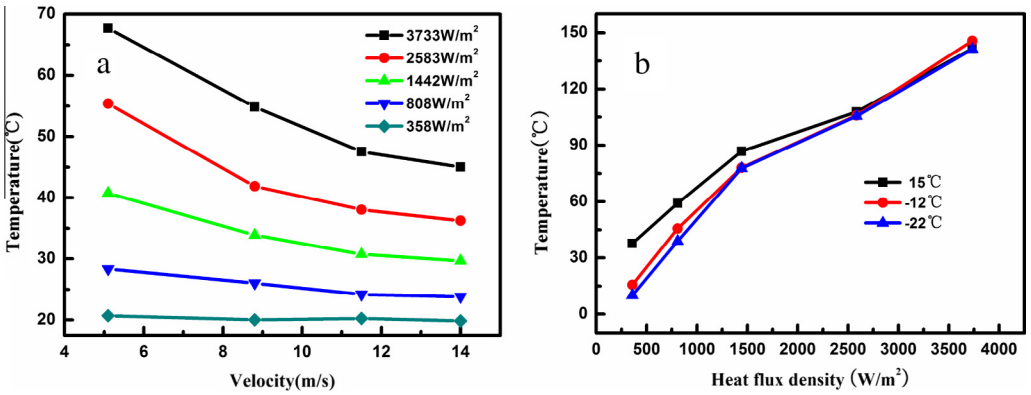

Fig. 7 – (a) The relationship between equilibrium temperature and wind speed at different heat flux densities. (b) The relationship between equilibrium temperature and heat flux density at different ambient temperatures. (A colour version of this figure can be viewed online.)

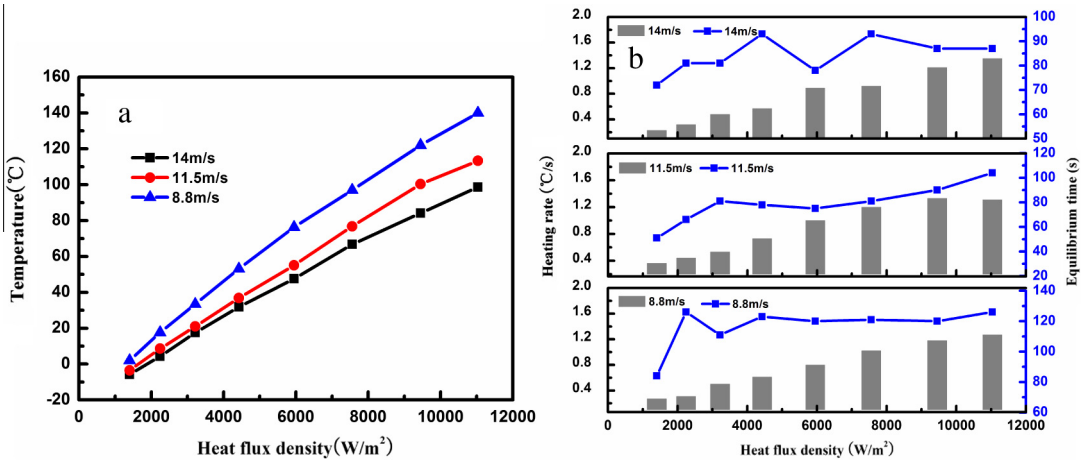

Fig. 8 – (a) The relationship between equilibrium temperature and heat flux density at different wind speed. (b) The contrast figures of the relationship between the heating rate and equilibrium temperature with heat flux density at different wind speed. (A colour version of this figure can be viewed online.)

is small although the fluctuation at the high heat flux density is bigger than at the low, which may cause by the uneven thickness of the resin layer on the CNP. In addition, 2D and 3D surface temperature distribution schematics at 3733 W/m^2 are described in Fig. 6(b) for the fluctuation is the largest in the line temperature distribution curves at this heat flux density. The temperature distribution is distinguished based on the color change in the photos. Obviously, most of the colors are yellow which means that the temperature on the overall surface has a relatively uniform distribution. As the analysis before, the resistance of the network can be described by a random resistor model, so that the uniform temperature distribution indicates these resistors have the similar resistance. That is, the tube-tube contact resistances are similar because these resistors can be viewed as a series circuit. Fig. S3(a) is the thermal radiation graph of PI-kanthal film composite and CGE. It is obvious that the surface temperature distribution of CGE is more even than PI-kanthal film composite from the color change. According to the line temperature distribution shown in Fig. S3(b), the fluctuation of CGE is much smaller than the PI-kanthal film composite. This non-uniformity affects the deicing performance when the sample in a strong convection effect and low surrounding temperature in practical application.

Cross section temperature distribution is achieved by the white cross hairs in the 2D image. The latitude and longitude distribution results are on the right side and at the below of the photo with the maximum temperature 136.12 and 125.85 °C, respectively. From the color distribution, a same conclusion that the tube-tube resistance along the thickness direction is similar can be obtained. Thus, the surface and cross section temperature distribution indicates that the material has a uniform electric heating performance.

The curves of equilibrium temperature versus the average surface wind speed of the CGE composite at different heat flux densities are presented in Fig. 7(a). The ambient temperature was 15 °C and the analysis area is also the rectangle of R4 in Fig. 6(b) with the wind direction paralleling the sample. The results show that the temperature values have a tiny variation at the low heat flux density such as 358 W/m^2. The trend demonstrates the heat generated at this heat flux density lower than the required energy of convection cooling at

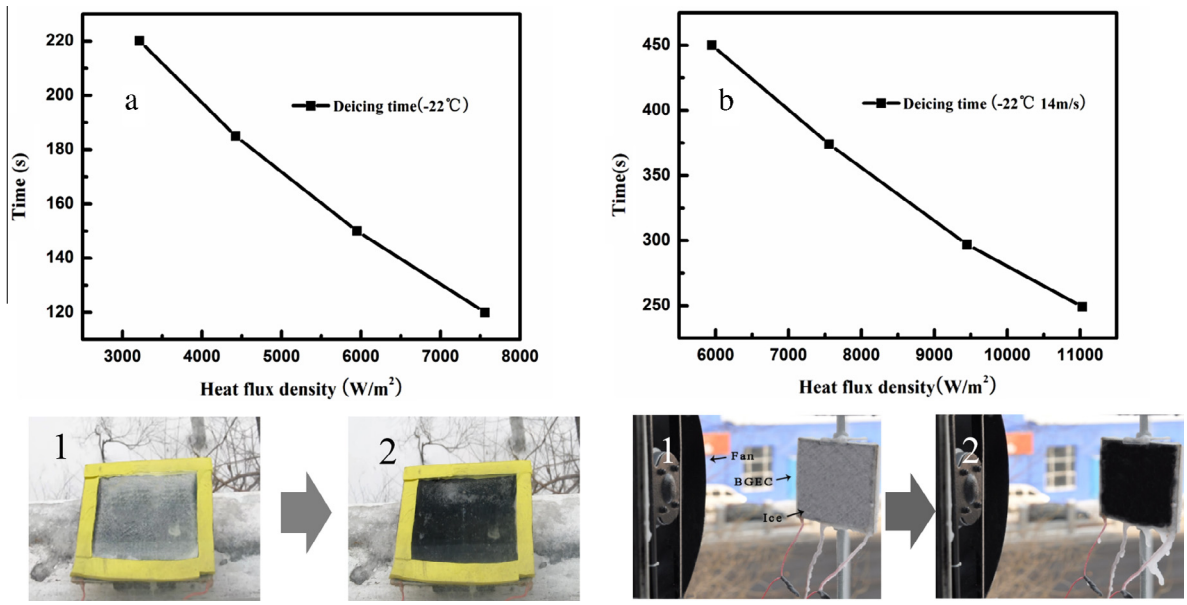

Fig. 9 – Ice thickness is 3 mm: (a) The relationship between the deicing time and the heat flux density at −22 °C of the surrounding temperature. (b) The relationship between the deicing time and the heat flux density at −22 °C of the surrounding temperature and 14 m/s of the average wind speed. (A colour version of this figure can be viewed online.)

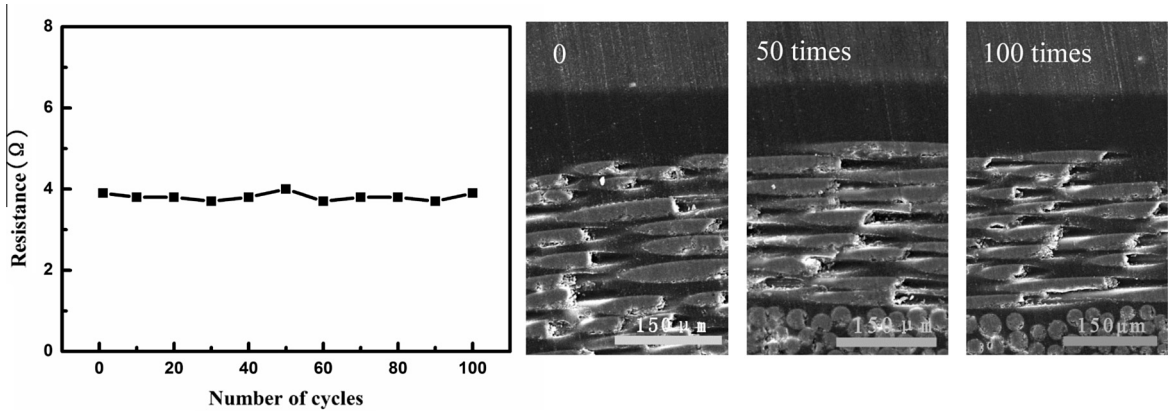

Fig. 10 – Resistance change between the electrodes of the CGE composite (left) and the cross section observation of the sample at 0, 50 and 100 times after heating–cooling cycle (right).

this wind speed. However, with increasing of the heat flux density, these curves illustrate an inverse functional relationship between the temperature and the wind speed. Under a same heat flux density, the equilibrium temperatures reduce markedly as the wind speed increases gradually, i.e. approximate 20 °C from 5.1 to 14 m/s at 3733 W/m^2. Meanwhile, a similar result can be obtained by comparing with the column chart of Fig. 5(b) investigated at windless condition which nearly reduce by 70 °C from windless to 14 m/s at 3733 W/m^2. This suggests that the convection effect emerges serious impact on reducing the surface temperature of CGE composite. Therefore, wind speed is the main factor affecting on deicing rate which needs to be considered significantly in practical application.

Fig. 7(b) reveals that the ambient temperature has a slight influence on the equilibrium temperature at the low heat flux density, for instance the equilibrium temperatures approximately increase by 30 °C when the ambient temperature varied from −22 to 15 °C at 358 W/m^2. Nevertheless, at the high heat flux density, such as 2583 and 3733 W/m^2, there are tiny changes of the equilibrium temperature. This phenomenon may be caused by two reasons; for one thing, the conduction cooling is slow between the electric heating layer and the surroundings, due to the epoxy layer on the surface of CNP; for another, the heating rate of CNP layer is high enough to make the speed of heat generated faster than the speed of heat conduction under the high heat flux density.

In order to study the coupling effect of the ambient temperature and wind speed influence on the equilibrium temperature, Fig. 8(a) presents the trend between the heat flux density and equilibrium temperature with various applied voltages (from 8 to 22 V) at −22 °C of the surroundings. It is obvious that heat flux density has a linear relationship to the equilibrium temperature at different wind speed. In

addition, with the increase of heat flux density, the equilibrium temperature gaps between different wind speeds are larger and larger. As described in the above analysis, the comparison results of the heating rate and equilibrium time with different wind speed at −22 °C of the ambient temperature are demonstrated in Fig. 8(b). Under a same wind speed, for example 8.8 m/s, heating rate increases markedly as the increase of heat flux density, nearly six times from 3733 to 11,033 W/m^2, and the similar results can be obtained from the other two speeds. Furthermore, the whole equilibrium times are less than 120 s and have a small change in the high heat flux densities, i.e. at 7588, 9450 and 11,033 W/m^2. The results suggest that CGE composite displays an excellent electric heating property, due to the unique transport mode of the electron in the CNP layer. Therefore, the CGE composite is a promising candidate as a self-heating material for deicing.

3.4. *Application in deicing of the CGE composite*

As for the application in the deicing of the self-heating composite, the investigation was carried out outdoor at −22 °C of the ambient temperature under windless condition. The ice thickness on the sample surface is 3 mm (36 g) controlled by adhering a tape with same thickness around the sample. The deicing time at various heat flux densities (voltage from 12 to 18 V) is demonstrated in Fig. 9(a). It is clear that the quantitative ice is melted to water completely in less than 220 s, which indicates the CGE composite has a high deicing rate, as presented from image 1 to image 2. As can be seen from the curve, the deicing time decreases dramatically with the increase of the heat flux density and the whole melting processes are in a short time at all heat flux densities. The energy consumption is 1332 kJ/m^2 in the process of deicing.

In order to verify the deicing effect of the CGE composite under the low ambient temperature and a certain wind speed, the relationship between the deicing time and the heat flux density under −22 °C of the ambient temperature and 14 m/s of the average wind speed on the sample surface are shown in Fig. 9(b). The deicing system is shown in the digital picture and the fan is the wind source providing a stable airflow on the ice layer (thickness is 3 mm).

As shown in the curve, with the heat flux density changing from 5950 to 11,033 W/m^2 (voltage from 16 to 22 V), it just takes approximately 450, 374, 297 and 249 s to melt the ice layer completely as presented from image 1 to image 2; the corresponding energy consumption in the case is 2758 kJ/m^2 more than two times compared with windless situation discussed in Fig. 9(a) which is caused by the convection effect between the sample and the airflow. Thus, the results indicate that the CGE composite is suitable for deicing in the coexistence condition of low temperature and wind such as in the fields of wind turbine blade and aircraft where require rapid deicing in a high efficiency.

Fig. 10 shows the structural stability of the resulting CGE composite characterized by a heating–cooling cycle outdoor for 100 times with a fluctuation temperature range from −22 to 120 °C on the surface of the sample and the resistance between the electrodes was measured intervals 10 times. Composite materials always are caused interface crack in the cycle of high and low temperature, especially for the electric heating materials, so as to affect the resistance of the composite. The result demonstrates stable resistance retention as its initial resistance after 100 cycles so that the CGE composite has an excellent structural stability for deicing in the heating–cooling cycle. The cross section micrographs corresponding to 0, 50 and 100 times after cycle were visualized with the FE-SEM as shown in Fig. 10. These images reveal the structure is not damaged between the layers after different cycle times. Hence, there are weak interface effects of the CGE composite and these layers contact tightly enough to bear the heating and cooling cycles repeatedly.

4. Conclusions

This work proposes a synthesizing method of meso/macropore CNP and a self-heating composite base on the CNP for the first time. The feasibility and efficiency of the self-heating composite for deicing were validated through experiments. This study resulted in the following conclusions:

The pore diameters of the meso/macropore CNP mainly distribute from 30 nm to 90 nm. The conductivity of CGE composite is 64.9 S cm^{-1} increasing nearly four orders of magnitude than the previous report. This self-heating composite provides excellent electric heating properties at ambient temperature ranging from 15 to −22 °C and wind speed from windless to 14 m/s with a rapid heating reaction and structure stability after heating–cooling cycles for 100 times. These properties indicate CGE composite can be employed as a highly efficient thermal source to generate stable heat for deicing.

With the increase of the heat flux density, the equilibrium temperature and the wind speed demonstrate an inverse function relationship and the ambient temperature has a slight influence on the equilibrium temperature at the low heat flux density. The deicing performance was investigated by melting a quantitative ice on the surface of the CGE composite at different heat flux densities under two conditions (−22 °C windless and −22 °C with 14 m/s of the wind speed), and the deicing times are less than 220 and 450 s, respectively. The excellent conductivity, electric heating performance and resistance stability of the CGE composite reported here suggest its potential utilization as a self-heating material for deicing in high efficiency.

Acknowledgements

This work is supported by the National Natural Science Foundation of China (Grant Nos.11225211, 11272106).

Appendix A. Supplementary data

Supplementary data associated with this article can be found, in the online version, at http://dx.doi.org/10.1016/j.carbon.2013.08.053.

REFERENCES

[1] Kim SY, Koretsky C. Effects of road salt deicers on sediment biogeochemistry. Biogeochemistry 2013;112(1–3):343–58.
[2] Novotny EV, Murphy D, Stefan HG. Increase of urban lake salinity by road deicing salt. Sci Total Environ 2008;406(1–2):131–44.
[3] Parent O, Ilinca A. Anti-icing and de-icing techniques for wind turbines: critical review. Cold Regions Sci and Technol 2011;65(1):88–96.
[4] Connor EF, Lee VY, Magbitang T, Hawker CJ, Volksen W, Siemens R, et al. First example of a nanoporous high-temperature polymer thermoset: eluding transition–time–temperature constraints associated with organic thermosets. Adv Mater 2004;16(17):1525–9.
[5] Susi T, Kaskela A, Zhu Z, Ayala P, Arenal R, Tian Y, et al. Nitrogen-doped single-walled carbon nanotube thin films exhibiting anomalous sheet resistances. Chem Mater 2011;23(8):2201–8.
[6] Park YT, Ham AY, Grunlan JC. Heating and acid doping thin film carbon nanotube assemblies for high transparency and low sheet resistance. J Mater Chem 2011;21(2):363–8.
[7] Zaeri MM, Ziaei-Rad S, Vahedi A, Karimzadeh F. Mechanical modelling of carbon nanomaterials from nanotubes to buckypaper. Carbon 2010;48(13):3916–30.
[8] Wu Z, Chen Z, Du X, Logan JM, Sippel J, Nikolou M, et al. Transparent conductive carbon nanotube films. Science 2004;305(5688):1273–6. 2004 August 27.
[9] Feng L, Li H, Li F, Shi Z, Gu Z. Functionalization of carbon nanotubes with amphiphilic molecules and their Langmuir–Blodgett films. Carbon 2003;41(12):2385–91.
[10] Ma W, Song L, Yang R, Zhang T, Zhao Y, Sun L, et al. Directly synthesized strong, highly conducting, transparent single-walled carbon nanotube films. Nano Lett 2007;7(8):2307–11.
[11] Dan B, Irvin GC, Pasquali M. Continuous and scalable fabrication of transparent conducting carbon nanotube films. ACS Nano 2009;3(4):835–43.
[12] Zhang X, Zhang J, Liu Z. Conducting polymer/carbon nanotube composite films made by in situ electropolymerization using an ionic surfactant as the supporting electrolyte. Carbon 2005;43(10):2186–91.
[13] Zakhidov AA, Suh D-S, Kuznetsov AA, Barisci JN, Muñoz E, Dalton AB, et al. Electrochemically tuned properties for electrolyte-free carbon nanotube sheets. Adv Funct Mater 2009;19(14):2266–72.
[14] Izadi-Najafabadi A, Yasuda S, Kobashi K, Yamada T, Futaba DN, Hatori H, et al. Extracting the full potential of single-walled carbon nanotubes as durable supercapacitor electrodes operable at 4 V with high power and energy density. Adv Mater 2010;22(35):E235–41.
[15] Cao Q, Kim H-S, Pimparkar N, Kulkarni JP, Wang C, Shim M, et al. Medium-scale carbon nanotube thin-film integrated circuits on flexible plastic substrates. Nature 2008;454(7203):495–500.
[16] Cao Q, Rogers JA. Ultrathin films of single-walled carbon nanotubes for electronics and sensors: a review of fundamental and applied aspects. Adv Mater 2009;21(1):29–53.
[17] Chen IWP, Liang Z, Wang B, Zhang C. Charge-induced asymmetrical displacement of an aligned carbon nanotube buckypaper actuator. Carbon 2010;48(4):1064–9.
[18] Brady-Estévez AS, Kang S, Elimelech M. A single-walled-carbon-nanotube filter for removal of viral and bacterial pathogens. Small 2008;4(4):481–4.
[19] Sears K, Dumée L, Schütz J, She M, Huynh C, Hawkins S, et al. Recent developments in carbon nanotube membranes for water purification and gas separation. Materials 2010;3(1):127–49.
[20] Meng C, Liu C, Fan S. Flexible carbon nanotube/polyaniline paper-like films and their enhanced electrochemical properties. Electrochem Commun 2009;11(1):186–9.
[21] Knight CC, Ip F, Zeng CC, Zhang C, Wang B. A highly efficient fire-retardant nanomaterial based on carbon nanotubes and magnesium hydroxide. Fire Mater 2013;37(2):91–9.
[22] Chen YW, Cheng CY, Miao HY, Zhang M, Liang R, Zhang C, et al. Application of response surface methodology in the optimization of laser treatment in buckypaper lighting for field emission displays. Int J Adv Manuf Tech 2013;64(1–4):515–36.
[23] Wang SK, Haldane D, Liang R, Smithyman J, Zhang C, Wang B. Nanoscale infiltration behaviour and through-thickness permeability of carbon nanotube buckypapers. Nanotechnology 2013;24(1).
[24] Wu QA, Bao JW, Zhang C, Liang RC, Wang B. The effect of thermal stability of carbon nanotubes on the flame retardancy of epoxy and bismaleimide/carbon fiber/buckypaper composites. J Therm Anal Calorim 2011;103(1):237–42.
[25] Zhuge JF, Gou JH, Chen RH, Zhou AX, Yu ZQ. Fire performance and post-fire mechanical properties of polymer composites coated with hybrid carbon nanofiber paper. J Appl Polym Sci 2012;124(1):37–48.
[26] Xu M, Futaba DN, Yamada T, Yumura M, Hata K. Carbon nanotubes with temperature-invariant viscoelasticity from –196 to 1000°C. Science 2010;330(6009):1364–8.
[27] Che J, Chen P, Chan-Park MB. High-strength carbon nanotube buckypaper composites as applied to free-standing electrodes for supercapacitors. J Mater Chem A 2013;1(12):4057–66.
[28] Dombovari A, Halonen N, Sapi A, Szabo M, Toth G, Mäklin J, et al. Moderate anisotropy in the electrical conductivity of bulk MWCNT/epoxy composites. Carbon 2010;48(7):1918–25.
[29] Moniruzzaman M, Sahin A, Winey KI. Improved mechanical strength and electrical conductivity of organogels containing carbon nanotubes. Carbon 2009;47(3):645–50.
[30] Kim YJ, Shin TS, Choi HD, Kwon JH, Chung Y-C, Yoon HG. Electrical conductivity of chemically modified multiwalled carbon nanotube/epoxy composites. Carbon 2005;43(1):23–30.
[31] Moisala A, Li Q, Kinloch IA, Windle AH. Thermal and electrical conductivity of single- and multi-walled carbon nanotube–epoxy composites. Compos Sci Technol 2006;66(10):1285–8.
[32] Bryning MB, Islam MF, Kikkawa JM, Yodh AG. Very low conductivity threshold in bulk isotropic single-walled carbon nanotube–epoxy composites. Adv Mater 2005;17(9):1186–91.
[33] Sandler JKW, Kirk JE, Kinloch IA, Shaffer MSP, Windle AH. Ultra-low electrical percolation threshold in carbon-nanotube–epoxy composites. Polymer 2003;44(19):5893–9.
[34] Byrne MT, Gun'ko YK. Recent advances in research on carbon nanotube–polymer composites. Adv Mater 2010;22(15):1672–88.
[35] Kaiser AB, Skakalova V. Electronic conduction in polymers, carbon nanotubes and graphene. Chem Soc Rev 2011;40(7):3786–801.
[36] Lu HB, Liu YJ, Gou JH, Leng JS, Du SY. Electrical properties and shape-memory behavior of self-assembled carbon nanofiber nanopaper incorporated with shape-memory polymer. Smart Mater Struct 2010;19(7):1–9.
[37] Lu HB, Liu YJ, Gou JH, Leng JS, Du SY. Synergistic effect of carbon nanofiber and carbon nanopaper on shape memory polymer composite. Appl Phys Lett 2010;96(8):084102-1–3.
[38] Mizuno K, Ishii J, Kishida H, Hayamizu Y, Yasuda S, Futaba DN, et al. A black body absorber from vertically aligned single-walled carbon nanotubes. Proc Natl Acad Sci 2009;106(15):6044–7.
[39] Liu P, Liu L, Jiang K, Fan S. Carbon-nanotube-film microheater on a polyethylene terephthalate substrate and its application in thermochromic displays. Small 2011;7(6):732–6.